

THE COSMOLOGICAL DENSITY AND IONIZATION OF HOT GAS: OXYGEN VI ABSORPTION IN QUASAR SPECTRA¹

SCOTT BURLES and DAVID TYTLER²

Department of Physics, and Center for Astrophysics and Space Sciences
University of California, San Diego
C0111, La Jolla, CA 92093-0111

ABSTRACT

We have conducted the first survey for Oxygen VI $\lambda\lambda 1032, 1038$ absorption lines in QSO spectra. We used medium resolution ($R \approx 1300$) high signal-to-noise (≈ 20) Faint Object Spectrograph spectra of 11 QSOs ($0.53 \leq z_{em} \leq 2.08$) from the Hubble Space Telescope Archive. We use simulated spectra to determine the significance of the line identifications, which lie exclusively in the Ly α forest.

We found 12 O VI doublets of which 9 are expected to be real and 6 constitute a uniform sample with both lines exceeding a rest equivalent width of $W_r = 0.21$ Å. The number of O VI doublets per unit redshift at a mean absorption redshift of $z_{ave} = 0.9$ is $\langle N(z) \rangle = 1.0 \pm 0.6$, which is similar to the density of C IV and Mg II absorbers.

In 7 of the 12 O VI systems, O VI, Ly β and C IV lines have similar equivalent widths, and are probably photoionized. In each of the remaining 5 systems, O VI has larger equivalent widths than those detected for Ly β and C IV. These systems are labeled as high ionization and are likely to be due to collisional ionization. These would be the first QSO absorption systems known to be collisionally ionized.

Assuming that the O VI lines are on the linear part of the curve of growth, we estimate the lower limit of the cosmological mass density, $\Omega(O\ VI) \geq 1 \times 10^{-8} h_{100}^{-1}$. Since O > O VI, if the mean cosmic metallicity, Z, were below 6×10^{-4} solar, then the accompanying Hydrogen and Helium would account for all baryons in the universe. We conclude that $\log Z(z = 0.9)/Z_{\odot} \geq -3.2$, and much greater if O VI is not the dominant ion of Oxygen.

Subject headings: cosmology – galaxy: intergalactic medium – galaxy: abundance – quasars: absorption lines

¹Based on observations obtained with the NASA/ESA Hubble Space Telescope obtained by the Space Telescope Science Institute, which is operated by AURA, Inc., under NASA contract NAS5-26555.

²scott@cass154.ucsd.edu, tytler@cass155.ucsd.edu

1. INTRODUCTION

We are interested in O VI absorption in QSO spectra because it is the easiest way to find cosmologically distributed hot gas with $T \approx 3 \times 10^5$ K. Such gas may have been missed from existing surveys of QSO absorption systems which require damped Ly α lines, Lyman continuum absorption, and Mg II or C IV lines. Unlike other QSO absorption systems, this hot gas might be collisionally ionized and could comprise the bulk of all baryons.

1.1. Source of Ionization

We are extremely interested in whether the O VI gas is photoionized or collisionally ionized. We consider collisional ionization because gas of the required temperatures exists, and there may be insufficient high energy photons for photoionization, especially at low redshifts ($z \leq 1$). We are also interested in the source of the ionizing energy – mechanical heating of the gas, or high energy UV photons.

Gas at temperatures needed to collisionally ionize O VI has been seen in galaxies, so we expect to see it in QSO absorption spectra. Pettini & D’Odorico (1986) have detected Fe X absorption from million degree gas in the Galactic halo and the Large Magellanic Cloud, while Davidsen et al. (1991) have seen O VI in absorption from gas in the our Galaxy’s halo along the direction to 3C273. High latitude clouds in our Galaxy produce shadows in the soft X-ray background (Burrows & Mendenhall 1991, Snowden et al. 1991) which reveal gas at $T \sim 10^6$ K in the halo of our Galaxy, and similar halos have been detected in other late-type galaxies (Wang 1991). But the X-ray halos of early-type galaxies are too hot – $5 - 23 \times 10^6$ K – to show strong metal lines in the HST wavelength range (Forman et al. 1979, Fabbiano 1989).

Photoionization is known to dominate in most QSO absorption systems which show strong C IV or Mg II (Bergeron 1988), but O VI is different. Photons with energies above 114 eV are needed to create O VI, and these are scarce because they are absorbed by both Hydrogen and Helium. QSOs and AGN are the likely sources of such photons. QSOs and AGN apparently do emit at these energies because they show strong O VI emission, and Ne VIII (>207 eV) emission lines are also common (Hamann, Zuo & Tytler 1995). But we do not know if this radiation escapes from the QSO environment, or from the host galaxies, which might be opaque in the He II continuum.

The He II Gunn-Peterson absorption provides a measure of the spectrum of the intergalactic background radiation field. The IGM He II/H I ratio depends on the flux of photons capable of ionizing He II to He III, and H I to H II. Jakobsen et al. (1994) find that the optical depth at He II 304 Å is $\tau(304) \geq 1.7$, which indicates that the spectrum of the radiation which ionizes the IGM is very steep. Madua (1994) detects little flux above 4 Rydberg, therefore even fewer photons exist above 114 eV.

We conclude that the hot gas may be similar to that in the halo of our Galaxy and collisionally ionized (e.g., Sembach & Savage 1992). It might be heated by gas cloud collisions and supernovae explosions which eject disk gas into the outer regions of the halo (e.g., Fan & Ikeuchi 1992, Shapiro & Benjamin 1991). Gas heated to a million degrees cools through radiative and dielectronic recombination on time scales of $t_c \sim 10^4 n_e^{-1} yr$, where n_e is the electron density (Shapiro & Moore 1976). The same O VI 2s–2p transition studied in this paper is responsible for the large cooling peak at $T \sim 10^5 K$ (Cox & Tucker 1969). To sustain collisionally ionized O VI absorption systems, the densities must be very low ($\ll 10^{-2} cm^{-3}$), or the heating sources must be very strong.

1.2. Density of Baryons in Hot Gas

Hot gas with strong O VI lines could be the largest portion of all baryons, exceeding the $\simeq 7\%$ in local stars and stellar remnants, and the $\simeq 7\%$ seen in cool gas as damped Ly α systems at $z \simeq 3$ (Wolfe et al. 1995). The missing baryons might be condensed (e.g. brown dwarfs, black holes), or diffuse hot ionized gas in clouds which are the subject of this paper. Gas which is hotter than $T \geq 10^6 K$ may be seen for the first time since O VI lines are then stronger than those of C IV (Verner, Tytler & Barthel 1994, hereafter VTB94).

The missing baryons could also be in the IGM, and too hot to show ultraviolet lines. COBE limits on the Compton distortion y parameter limit the temperature and density of a hot and dense IGM, but even if all baryons were in the IGM, the maximum temperature is still a few keV (few $10^7 K$; Wright et al 1994; Barcons, Fabian & Rees 1991), which is still too hot to show UV absorption lines.

Many of the missing baryons could be in gas which is cooler. O VI is most prevalent at $T = 3 \times 10^5 K$ (VTB94). By $10^6 \leq T \leq 4 \times 10^6 K$ O VI lines will be stronger than those from C IV or N V, and for highest temperatures C IV and N V will not be visible at all (VTB94). We will only see the part of the hot gas which is enriched with metals, This could include most hot gas if the heating is associated with supernovae, galaxy formation and mergers, and if all galaxies enrich the gas in their surroundings as occur in clusters.

1.3. Past Searches

Although there have been no traditional surveys for individual O VI lines in QSO spectra because of severe blending of lines in the Ly α forest, the following absorption line studies have observed O VI and provide strong evidence that O VI absorption is both real and common.

Hartquist & Snijders (1982) showed that O VI is common in absorption systems which are very close to QSOs, the “associated” C IV systems. Tytler & Barthel (unpublished) found that most associated systems with strong C IV lines ($W_r(CIV) \geq 5 \text{ \AA}$) have O VI, and O VI is also

common in BAL systems (Hamann et al. 1995). In all these cases the O VI is strong because the absorbers are near individual QSOs. Therefore the gas is probably photoionized, which shows that many QSOs do emit above 114 eV. This radiation does escape into the QSO’s galaxy, but not necessarily into the IGM.

Lu & Savage (1993) formed a single composite spectrum of the absorption lines from typical high redshift ($z_{abs} \simeq 2.8$) absorption systems which show relatively strong C IV lines. They found O VI in systems which had C IV, but they could not determine the fraction of C IV systems with O VI. Some had low ionization lines, while others did not. They did not detect N V lines, and deduced $N(\text{O VI})/N(\text{N V}) \geq 4.4$, which implies $T \geq 2.5 \times 10^5$ K for collisional ionization.

Bahcall et al. (1993) note that O VI is seen in three of the metal line systems in their HST quasar spectra, one of which was an associated absorber. Bergeron et al. (1994) note that 4 of 5 metal systems show O VI, but they are unable to determine if the gas is collisionally ionized or photoionized. These results all suggest that O VI systems are as common or more common than C IV systems (several per QSO). We will now determine how common.

First we show that we can identify O VI doublets in the Ly α forest. We choose to work with HST UV spectra because the forest is less dense at the lower redshifts of HST spectra compared to the higher redshifts visible from the ground. We measure the frequency of O VI systems, and we try to determine the level of ionization, and whether the gas is photoionized or collisionally ionized. Finally we estimate the contribution that hot gas makes to the cosmological mass density of baryons.

2. OXYGEN VI SEARCH

The Hubble Space Telescope Archive provides a resource to search for O VI absorption. In particular, the medium resolution ($R \approx 1300$) gratings of the Faint Object Spectrograph have both the sensitivity and the resolving power to identify weak metal lines in absorption. Spectra are chosen by the QSO properties (magnitude and redshift), gratings, and exposure time. Since the search for O VI is done exclusively in the Lyman- α forest, high signal-to-noise is necessary.

To ensure the reality of O VI absorption, strict rules are applied to line lists. These rules incorporate measured wavelength, equivalent width, and 1σ errors. Once the ground rules are determined, a computer algorithm is responsible for identifying systems which exhibit O VI absorption. We use a computer to automatically find O VI and to maintain objectivity and repeatability. Physical significance is measured by applying the same rules to false sets of rest wavelengths and comparing results with the true set.

2.1. Processing the HST Spectra

We consider spectra from only the FOS high resolution gratings G130H, G190H and G270H. The G160L does not have enough resolution, and there were no suitable GHRS G140L spectra. Table 1 shows the 11 QSOs chosen for the O VI search. Most of the spectra are from the G190H or G270H gratings, because few G130H spectra have adequate S/N. There are 8 steps prior to the O VI search,

1. We use the following rules to ensure that the z_{em} of each QSO is sufficient to place O VI well onto the FOS gratings:

$$z_{em} \geq \begin{cases} 0.3 & \text{for G130H} \\ 0.65 & \text{for G190H} \\ 1.25 & \text{for G270H.} \end{cases}$$

2. We obtained each spectrum and its error array from the HST Archive.
3. Coadd spectra which have multiple exposures.
4. Find all the absorption lines from the interstellar medium of our Galaxy. We shift each spectrum so that these lines give a mean velocity of zero (Schneider et al. 1993). We list the offsets added to each spectrum in Table 1.
5. Fit a continuum to each spectrum manually. Due to the subjectivity of continuum fitting, the systematic errors introduced in the measured equivalent widths are difficult to calculate. However, we assume that other errors in our final results greatly outweigh the errors in the continuum fits.
6. Convert the spectrum and its error array into a spectrum which gives the minimum equivalent width of unresolved lines of specified significance level.
7. Find all 5σ lines in a spectrum. There are typically 40 – 80. Measure their equivalent widths W , $\sigma(W)$, and wavelengths.
8. Search the literature for all known absorption systems. Identify lines which belong to these systems, and remove them from the sample in which we will search for O VI.

2.2. Search for O VI Lines

There are no published systematic searches for individual spectral lines in the Ly α forest region because the large number of forest lines and the high incidence of line blending lead to numerous false identification. We require a search which has the desirable attributes of a medical screen for a rare disease: (1) high sensitivity to minimize the number of missed O VI systems (false negatives), and (2) high specificity to minimize the number of false positive identifications. We

use a computer code to increase the sensitivity, accuracy, completeness and speed of the survey, and use rules to limit the number of false positives to about 20% of the sample. We would prefer to have fewer false positives, but this is only possible if we consider just the very strongest lines. Then we miss most O VI lines, and we cannot estimate their overall frequency.

False identifications can be noise features, or real lines with other identifications, especially Ly α . We use three criteria to limit the number of false identification: line significance, redshift agreement, and equivalent width ratios. In all detections, both O VI lines must be detected above the 2σ equivalent width limit. Furthermore, their measured equivalent width ratio must lie within 1σ of the theoretical boundaries.

The procedures we use to find O VI lines in certain and possible redshift systems are described below.

2.2.1. Search for O VI Lines in Certain Redshift Systems

In published, or new metal line systems (e.g. with Mg II, C IV or Lyman limits) which are considered certain, we look for 2σ O VI lines. There are about 0 – 3 such systems per QSO, so the chance of false positive identification of both O VI lines is $\leq 3\%$ per QSO. We measure lines associated with the absorption systems and calculate the mean redshift, which can vary from the published absorption redshift because of wavelength offsets. We identify all additional lines, including O VI, which match the criteria of the next section.

2.2.2. Search for O VI Lines in Uncertain Redshift Systems

We use the following procedure to find interesting lines, identify possible new redshift systems and then reject unreasonable ones.

1. We search for all systems with at least two 5σ lines from Ly α , Ly β , Ly γ or O VI. Lines are accepted into a system if their redshift differs from the weighted mean z_{ave} by less than 0.0005 ($\sim 80 \text{ km s}^{-1}$), which is sufficient to include 93% of lines in metal systems identified by Bahcall et al. (1993). The weighted mean z_{ave} is defined as

$$z_{ave} \equiv \frac{\sum_i w_i^2 z_i}{\sum_i w_i^2},$$

where w_i is the weight placed on the redshift of each line:

$$w_i = \begin{cases} \frac{W_{obs}}{\sigma(W)} & W_{obs} < 0.79 \text{ FWHM} \\ \frac{0.79 \text{ FWHM}}{\sigma(W)} & W_{obs} \geq 0.79 \text{ FWHM} \end{cases},$$

where FWHM is the spectral resolution of each grating in Å. We define the equivalent width cut-off as the limit for unsaturated lines. Once a line becomes saturated, the accuracy of the line center depends only on the S/N of the spectrum. Lines which exceed the saturation criterion are marked in Table 4.

2. We calculate expected positions of the remaining lines in these system, and we measure wavelengths and equivalent widths, or limits for these lines.
3. We search for additional identifications for the new 2σ lines amongst all systems with at least two 5σ lines.
4. As a further constraint, we use the ratios

$$R_{H\ I} = \frac{W(1215)}{W(1025)},$$

and

$$R_{O\ VI} = \frac{W(1032)}{W(1038)}.$$

If Ly β (1025) or O VI(1038) is not present, then the ratios are calculated using the 2σ equivalent width limits. A ratio is judged acceptable if it falls between $1 - \sigma(R)$ and $2 + \sigma(R)$ for O VI, and $1 - \sigma(R)$ and $5.27 + \sigma(R)$ for H I, where $\sigma(R)$ is the error on the ratio obtained from the errors on the individual W values, and the numerical values are for unsaturated and saturated lines. We discard systems which do not have at least one acceptable ratio.

We wrote a computer code to follow the above procedures, and we ran this code with both true and false rest wavelengths. The false wavelengths did not have the same ratios as the true wavelengths of any strong lines. We then counted the number of O VI systems identified with both true and false wavelengths. The above procedures were then adjusted to give a true/false ratio of 5:1. We also ran tests with true rest wavelengths and random absorption line positions, which gave the same result.

Unfortunately, we did not accept lone O VI lines, because the number of false identifications was similar to the true number. In figure 1, we show the number. Our simulations show that we must insist that all systems have ≥ 3 lines to keep the expected number of false O VI identifications < 1 per spectrum. Simulations indicate that Ly α should be stronger than O VI in either collisional or photo- ionization (VTB94), so we use lines of the Lyman series to confirm O VI identifications. Although we exclude possible O VI detections, it is necessary to detect a third line to keep false identifications to a minimum. A Lyman line must be detected at the O VI redshift with the following stipulations:

1. If Ly α exists and $R(H)$ is acceptable, then the system is accepted.

2. If $\text{Ly}\beta$ exists without a $\text{Ly}\alpha$, the system is discarded.
3. If $\text{Ly}\beta$ exists and has an acceptable equivalent width ratio with $\text{Ly}\gamma$, and $\text{Ly}\alpha$ cannot be checked, the system is accepted.

No method will throw out all false systems and keep all real ones. For example, consider pairs of 5σ lines which are identified as $\text{Ly}\alpha$ and $\text{Ly}\beta$. Simulations show that such pairs do occur commonly, even in HST spectra at low z : we expect 2 false pairs of 5σ lines in every QSO. But in real data we see about 6 such $\text{Ly}\alpha - \text{Ly}\beta$ pairs per QSO, so 67% are real. We look for 2σ O VI lines in each such system.

3. FREQUENCY OF OXYGEN VI

In Table 2, we list the number of O VI systems identified with three different sample criteria. In Sample A, the absorption system identified with O VI must have at least three lines with a redshift within $\Delta z = 0.0005$ of the weighted mean redshift of the system. All lines must have a significance level $\geq 2\sigma$. Sample B is a subset of A where at least two of the lines must have a significance level of $\geq 5\sigma$. Sample C is a subset of A, with the constraint that both lines of the O VI doublet must have a rest equivalent width $W_{rest} \geq 0.21 \text{ \AA}$, which is the minimum 2σ rest equivalent width which could be seen in all the spectra. Sample C is the most stringent and complete sub-sample and will be used to measure the density of O VI systems.

Also shown in the same table is the number of O VI identifications per object using false rest wavelengths. Simulations were run with 10 sets of false wavelengths for $\text{Ly}\alpha$, $\text{Ly}\beta$, $\text{Ly}\gamma$ and O VI. We used the same criteria as with the real wavelengths. The average number of false identifications is shown in the table, and gives an estimate of the number of identifications in the true sample which are due to chance.

Samples A and B differ by less than we expected, because there is only one system in A that does not satisfy the requirements of B. But A contains twice as many false IDs as B, so B is a significantly cleaner sample. The line density is actually higher in B than A, but the difference is not significant.

With 11 objects in this preliminary survey, we can estimate the number of O VI absorbers per unit redshift.

$$N(z) = \frac{\text{Total True} - \text{Total False}}{\Delta z_{tot}}$$

where

$$\sigma_N(z) = \frac{\sqrt{\text{Total True} + \text{Total False}}}{\Delta z_{tot}}$$

where $\Delta z_{tot} = 4.73$.

Table 3 contains system number densities for a variety of absorption systems. The first three are our samples of O VI, and the fourth is a sample of Ly α –Ly β pairs in which we found $W(1025) \geq 0.30\text{\AA}$. For comparison with other samples, we use Sample C, which is most complete. At low z systems with O VI are as common as the other main types of system: Mg II, C IV and LLS.

3.1. Individual Systems with O VI

Table 4 shows the twelve systems of Sample A. For each of these systems we searched for all other strong lines which would appear in the observed wavelength range, including: C IV 1548, 1550, N V 1238, 1242, Si III 1206, Si II 1190, 1193, 1260, Si IV 1393, 1402, N III 989, C III 977, and C II 1334. Two of these systems show H I and O VI only, but all the others show at least one other element, and have ≥ 5 lines each. Lines are accepted into a system if their redshift is within ± 0.0005 of the weighted mean.

In Figure 2 we show the absorption line positions on the HST spectra. Note that the Ly β , O VI(1032) and O VI(1038) lines form a well resolved uniformly spaced triplet, which helps visual identifications.

For each of the 12 O VI systems of Sample A, Figure 3 shows enlarged plots of Ly α , Ly β , O VI and C IV all on a velocity scale given by the listed mean redshift. We do not show lines which are below 2σ significance. Line widths are all set by the FOS resolution. Comments on individual systems are in the appendix.

3.2. Contamination of O VI(1038)

Lu & Savage (1993) point out that O VI 1037.62 can be contaminated by C II 1036.34 and O I 1039.23, especially in low ionization systems.

Lines O VI(1038) and C II(1036) are separated by $\Delta\lambda = 1.32$ so to resolve these lines we need spectra with resolution $R \geq 785$. The FOS high resolution spectra have $R \approx 1300$ so we would expect, assuming usual b parameters $\leq 75 \text{ km s}^{-1}$, that these lines should be resolved in this survey. We do just resolve these lines, and we fitted each to get their individual equivalent widths which are listed in Table 5.

As a check we measured lines C II 1334.53 and O I 1302.17 which should both be stronger than the contaminants C II 1036.34 and O I 1039.23 because their λf values are larger by 1.3 and 6.6 times respectively. We follow this procedure:

1. Measure width of C II(1334).
2. Calculate line width of C II(1036) with ratio of oscillator strengths, assuming lines are linear.

3. Measure total width from 1036–1038 Å.
4. Subtract calculated C II(1036) from the combined width of step 3

In Table 5, we list the equivalent widths of O VI(1032), O VI (1036-1038) and C II(1334). The O VI 1036-1038 widths in Table 5 includes both O VI and C II, whereas those in Table 4 are for O VI alone. We detect C II(1334) in four O VI systems, and for each of these systems, we subtract $W(\text{C II}, 1036)$ from $W_r(1036-1038)$ to calculate the "subtracted" doublet ratio. If absorption is due to O VI and C II alone, this would provide the correct width of O VI(1038). For all the systems of Sample A, both the fitted and subtracted doublet ratios fall within the allowed 1σ errors. The fitting procedure contains less steps and is subject to less uncertainty than the subtracting procedure. Since the spectra of this survey have adequate resolution to separate C II(1036) and O VI(1038), we conclude that the measured widths and ratios obtained by fitting O VI and C II (Table 4) independently are more accurate.

The other possible contamination due to O I is ruled out. O I $\lambda 1302$ was not detected in any systems associated with O VI. So the contribution from the weaker O I(1039) is safely assumed negligible.

3.3. Column Densities and Velocity Dispersions

We employ the doublet ratio method to estimate column densities and velocity dispersions where possible. Table 6 shows our calculations for O VI, C IV, and H I in systems where two or more ions are present. We calculate the 1σ errors in Table 6 by allowing the equivalent widths to assume any value with their 1σ errors and taking the extreme results as limits. This is an over estimation of the random errors which partially compensates for the systematic errors of measuring equivalent widths of unresolved lines in the Ly α forest. Wavelengths and f-values used in the column density calculations were taken from Morton (1991).

As seen from Table 6, our search was only sensitive to column densities $\log(N) > 14.4$. This is consistent with the minimum equivalent width threshold, $W_r = 0.21$ Å. Figure 4 shows the allowable column densities of a single component for a given doublet ratio. Our survey of O VI is not sensitive to *linear* single component absorbers. High velocity dispersion ($> 100 \text{ km s}^{-1}$) is strong evidence for multiple absorbers in the system.

3.4. Collisional or Photo- ionization?

HST FOS spectra do not have enough spectral resolution to give accurate column densities and velocity dispersions, so it is difficult to determine if the gas is photoionized or collisionally ionized. So we use the relative strengths of the O VI, C IV, and Ly β lines to indicate the level of

ionization. We define two equivalent width ratios:

$$R_{OB} = \frac{O\ VI(1032)}{Ly\beta},$$

and

$$R_{OC} = \frac{O\ VI(1032)}{C\ IV(1548)}.$$

In Table 7 we give values for these ratios. $Ly\beta$ is seen in 11 systems, and C IV in 8.

Seven out of the eight systems in which C IV and O VI are detected have similar ratios: $R_{OC} < 1.2$ and $R_{OB} < 1$ corresponding to medium ionization. Although C IV and O VI are both detected, C IV is the dominant ion and the system should be labeled as such. Five of the seven medium ionization systems exhibit multiple low ionization lines (i.e. C II, C III, N III, Si II, Si III). The ionization energies in each of the five systems range from 11eV to 114eV. Such a wide range of ionizations, and therefore a large variety of ions, cannot be modeled with pure collisional ionization in a single simple cloud. As was restated by Verner and Yakolev (1990), the large variety of ions found in absorption systems is strong evidence that power law ionizing radiation is present. The eighth system, at $z_{abs} = 1.08$ of PG 1206+4557, has $R_{OC} = 4.17$ and $R_{OB} = 2.02$. This system has significantly different values and is classified as high ionization. Only collisional ionization at high temperatures, $T > 10^5 K$, or extreme photoionization, $\chi > 0.1$, can produce the measured ratios (χ is the ratio of the number of photons with energies above the Lyman edge to the number of particles). Since C IV is so weak and N V is undetected, we believe that the system is collisionally ionized.

In the remaining four systems in which O VI was detected, none had a corresponding C IV detection. Each was assigned an upper limit 2σ equivalent width associated with the non-detection of C IV. These systems are marked on Figure 5 with arrows starting at the lower limit of the ratio. In the system $z_{abs} = 0.746$ of PKS 1424-1120, neither C IV nor $Ly\beta$ are detected and a lower limit is assigned for each ratio. These systems are labeled as high ionization since O VI is the dominant metallic ion.

3.5. Cosmological Mass Density

The cosmological mass density $\Omega_{OVI}(z)$ of O VI is defined as the comoving mass density of O VI in terms of the current critical density.

$$\Omega_{OVI} = \frac{m_{OVI}}{\rho_c c H_o^{-1}} \frac{\sum_i N_i(OVI)}{\sum_i \Delta X_i},$$

where m_{OVI} is mass of the Oxygen ion, ρ_c is the current critical density, H_o is the current Hubble parameter, $N_i(OVI)$ is total O VI column density towards the i th QSO over an absorption path distance ΔX_i defined as

$$\Delta X = \begin{cases} \frac{1}{2} \{[(1 + z_{max})^2 - 1] - [(1 + z_{min})^2 - 1]\} & (q_0 = 0), \\ \frac{2}{3} \{[(1 + z_{max})^{3/2} - 1] - [(1 + z_{min})^{3/2} - 1]\} & (q_0 = 0.5). \end{cases}$$

Using values of the redshift range in Table 2,

$$\sum_i \Delta X_i = \begin{cases} 9.24 & (q_0 = 0), \\ 6.60 & (q_0 = 0.5). \end{cases}$$

The standard error of the mass density is estimated as

$$\sigma_\Omega = \frac{1}{(1 - \frac{1}{m})^{1/2}} \frac{\sqrt{\sum_i [N_i(OVI) - \langle N(OVI) \rangle]^2}}{\Delta X_{tot}},$$

where m is the total number of absorption systems in the sample, and $\langle N(OVI) \rangle$ is the mean column density of the sample.

Lower limits of the column density in each absorption system are calculated with the assumption that the O VI absorption features are unsaturated. The column density of the absorber is then proportional to the rest equivalent width (Spitzer 1978)

$$N(cm^{-2}) = \frac{1.13 \times 10^{20} W(\text{\AA})}{\lambda^2(\text{\AA}) F_{ij}},$$

where F_{ij} is the oscillator strength of the transition λ is the rest wavelength of the transition W is the rest equivalent width. The absorption features of O VI $\lambda 1038$ are weaker and less saturated. Using the six systems of Sample C and the rest equivalent width of O VI(1038), we obtain

$$\sum_i N_i(OVI) \geq 5.9 \times 10^{15} cm^{-2}.$$

We arrive at an estimate for the cosmological mass density of O VI at $z_{ave} = 0.9$,

$$\Omega_{OVI} \geq \begin{cases} 1.4 \pm 0.4 \times 10^{-8} h^{-1} & (q_0 = 0), \\ 2.0 \pm 0.6 \times 10^{-8} h^{-1} & (q_0 = 0.5), \end{cases}$$

where $H_o = 100h \text{ km s}^{-1} \text{ Mpc}^{-1}$.

3.6. Limit on Cosmic Metallicity

It is now straightforward to place a lower limit on the mean cosmological metallicity at $z_{ave} = 0.9$. If the cosmic metallicity is too low, all the baryons in the universe are needed to

account for the O VI seen in this survey. Let $\zeta(z)$ be defined as the ratio of mean metallicity at redshift z to the solar metallicity,

$$\zeta(z) = \mu \left(\frac{H}{O} \right)_{\text{Solar}} \left(\frac{O}{\text{OVI}} \right) \frac{\Omega_{\text{OVI}}(z)}{\Omega_b}$$

where μ is the mean molecular weight, which equals 1.3 for a mixture of 25% Helium and 75% Hydrogen by mass; $(H/O)_{\text{Solar}} = 1174.9$ (Anders & Grevesse 1989); and Ω_b is the cosmological baryon mass density. The ionization fraction O/O VI is impossible to calculate for each absorption system with the current data, but a lower limit is placed on the metallicity by assuming O/O VI = 1. A recent measurement of deuterium at high redshift by (Tytler & Fan 1994) yields $\Omega_b^{-1}(z) = 0.023h^{-2}$.

$$\zeta(z) \geq \begin{cases} 8.9 \pm 2.7 \times 10^{-4}h & (q_0 = 0), \\ 1.4 \pm 0.4 \times 10^{-3}h & (q_0 = 0.5). \end{cases}$$

The calculation is subject to small number statistics, and we can estimate the sensitivity of the lower limit by removing one system of Sample C. If we discard the system with the largest equivalent width ($z_{\text{abs}} = 0.927$ towards 1206+4557), the lower limit is reduced by 35%. The calculated lower limit is a safe estimate for the following reasons: We have assumed that all Oxygen at $z_{\text{ave}} = 0.9$ is in the form of O VI, that all absorption is linear, and that we have detected all O VI along the absorption path.

4. SUMMARY

O VI absorption is as common at $z_{\text{ave}} = 0.9$ as C IV and Mg II absorption. Using a minimum rest equivalent width of $W_r = 0.21 \text{ \AA}$ and accounting for the average number of chance coincidences per spectra, the number density of O VI absorbers per redshift is

$$\langle N_{\text{OVI}}(z = 0.9) \rangle = 1.0 \pm 0.6 .$$

Using a systematic computer search, we found 12 redshifts with $\geq 2\sigma$ equivalent widths at O VI wavelengths. The O VI systems were categorized as either medium or high ionization, Seven systems are medium ionization, with 5 showing multiple low ionization lines. The 5 high ionization systems have O VI stronger than both C IV and Ly β .

We summed over all O VI absorption with widths above the threshold $W_r > 0.21 \text{ \AA}$ to estimate the cosmological mass density at $z = 0.9$. Since we could not resolve velocity structure, we calculated a lower limit by assuming linear absorption,

$$\Omega_{\text{OVI}} \geq \begin{cases} 1.4 \pm 0.4 \times 10^{-8}h^{-1} & (q_0 = 0), \\ 2.0 \pm 0.6 \times 10^{-8}h^{-1} & (q_0 = 0.5). \end{cases}$$

We proceed further by assuming all Oxygen is in the form of O VI and place a lower limit on the metallicity in solar units at $z = 0.9$,

$$\zeta(z) \geq \begin{cases} 8.9 \pm 2.7 \times 10^{-4} h & (q_0 = 0), \\ 1.4 \pm 0.4 \times 10^{-3} h & (q_0 = 0.5). \end{cases}$$

The survey for hot gas, such as O VI, must be pursued in the future. In addition to better statistics at low redshift, the survey should be extended to high redshift to measure changes in the abundance of hot gas. Ions with higher energies, such as Ne VIII and Mg X, should be studied. The launch of the Hubble Space Telescope has allowed us to quantify the amount of 100 eV intergalactic gas for the first time.

We are grateful to Chris Davis for assisting in the reduction of the archived HST spectra.

QSO(1950)	Name	z_{em}	V	FOS Grating	Offset(\AA)	Exposure (s)
0122-0021	PKS 0122-00	1.070	16.70	190H	+1.3	3000
				270H	+0.8	720
0454-2203	PKS 0454-22	0.534	16.1	130H	0.0	6500
				190H	0.0	5900
				270H	0.0	2000
1206+4557	PG 1206+459	1.158	15.79	190H	+0.8	4500
				270H	+0.9	1000
1317+2743	Ton 153	1.022	15.98	190H	+1.5	4500
				270H	+1.4	1000
1352+0106	PG 1352+011	1.121	16.03	190H	+2.3	5300
				270H	+1.6	1150
1407+2632	PG 1407+265	0.944	15.73	190H	+1.5	4250
				270H	+1.9	1125
1424-1150	PKS 1424-11	0.806	16.49	190H	+1.5	6600
				270H	+1.7	1900
1435+6349	S4-1435+63	2.068	15.0	270H	0.0	3200
1522+1009	PG 1522+101	1.321	15.74	190H	+0.6	9500
				270H	+1.9	2650
1634+7037	PG 1634+706	1.334	14.90	190H	+0.9	5300
				270H	+0.7	6750
2340-0340	PKS 2340-03	0.896	16.02	190H	+0.2	4100

Table 1: List of Quasar Spectra

Object	Lyman- α, β		O VI(1032,1038)						Redshift	Minimum
	True ID	False ID	True ID			False ID			Range (Δz)	Observed Width(\AA)
			A	B	C	A	B	C		
0122-0021	5	2.2	2	2	2	0.2	0.1	0.0	0.61–1.07	0.31
0454-2203	4	0.7	1	1	1	0.4	0.1	0.1	0.31–0.53	0.28
1206+4557	6	1.1	3	2	2	0.2	0.2	0.1	0.61–1.16	0.24
1317+2743	2	0.6	0	0	0	0.3	0.2	0.1	0.61–1.02	0.21
1352+0106	5	1.1	1	1	1	0.3	0.3	0.2	0.61–1.12	0.23
1407+2632	6	0.3	0	0	0	0.1	0.1	0.1	0.61–0.94	0.31
1424-1150	2	0.1	2	2	0	0.0	0.0	0.0	0.61–0.81	0.29
1435+6349	0	0.6	0	0	0	0.7	0.2	0.2	1.61–2.08	0.23
1522+1009	2	0.6	0	0	0	0.7	0.4	0.3	0.61–1.32	0.16
1634+7037	1	0.2	2	2	0	0.4	0.1	0.1	0.75–1.33	0.17
2340-0340	3	0.4	1	1	0	0.2	0.1	0.1	0.61–0.90	0.25
Total	39	7.9	12	11	6	3.5	1.8	1.3	4.73	

Table 2: Frequency Of Absorption Systems with O VI Doublets

A: System must have at least three lines with a redshift within $\Delta z = 0.0005$ of the mean redshift of the system. All lines must be $\geq 2\sigma$.

B: Subset of A where at least two lines are $\geq 5\sigma$.

C: Subset of B where both O VI lines have a rest equivalent width $\geq 0.21 \text{ \AA}$.

Ion	Sample	True	False	\bar{z}	N(z)	ref
		Low	Redshift			
O VI	A	12	3.5	0.9	1.8 ± 0.8	1
	B	11	1.8	0.9	1.9 ± 0.7	1
	C	6	1.3	0.9	1.0 ± 0.6	1
HI	Ly α -Ly β	39	8	0.9	6.5 ± 1.4	1
HI	Ly α	W(1215) > 0.32Å		0.7	21.8 ± 2.1	2
HI	LLS	$\tau > 0.4$		0.9	1.1 ± 0.3	2
C IV	W(1548) > 0.30Å			0.3	0.87 ± 0.43	2
Mg II	W(2796) > 0.60Å			0.5	0.26 ± 0.08	3
Mg II	W(2796) > 0.30Å			0.9	1.0 ± 0.25	4

Table 3: Number Density Of Various Absorption Systems

References. — (1) This Paper; (2) Bahcall et al. 1993; (3) Tytler et al. 1987; (4) Fan 1995.

Table 4. Oxygen VI System Line List^a

Wavelength (Å)	ID	z_{obs}	W_{obs} (Å)	$\sigma(W)$ (Å)	SL ^b	LR ^c
0122-0021		$z_{em} = 1.070$		V=16.1 ^d		
1	$z_{ave} = 0.95336, \sigma_z = 0.00031$ A,B,C ^e					
2374.84	Ly α	0.95352	2.368	0.205 ^f	11.55	1.73
2003.88	Ly β	0.95363	1.367	0.102 ^f	13.38	2.19
1900.05	Ly γ	0.95370	0.623	0.122	5.11	
2015.31	OVI(1032)	0.95295	1.211 ^g	0.098 ^f	12.31	1.41
2026.92	OVI(1038)	0.95343	0.861	0.095	9.03	
1908.48	CIII(977)	0.95337	1.395	0.118 ^f	11.82	
1933.90	NIII(989)	0.95383	0.694	0.102	6.80	
2356.67	SiIII(1206)	0.95331	0.467	0.200	2.35	
	NV(1238)		$\leq 0.410^h$			
	NV(1242)		$\leq 0.410^h$			
2606.32	CII(1334)	0.95298	0.360	0.154	2.33	
3024.09	CIV(1548)	0.95329	1.989	0.180 ^f	11.05	1.13
3029.12	CIV(1550)	0.95330	1.763	0.180 ^f	9.79	
2	$z_{ave} = 0.96686, \sigma_z = 0.00031$ A,B,C ^e					
2391.13	Ly α	0.96693	1.873	0.202 ^f	9.29	2.33
2017.20	Ly β	0.96662	0.804	0.098	8.22	0.58 ⁱ
1912.64	Ly γ	0.96664	1.394	0.116 ^f	12.04	
2030.11	OVI(1032)	0.96730	0.708	0.095	7.47	1.45
2041.14	OVI(1038)	0.96714	0.488	0.093	5.25	
	NV(1238)		$\leq 0.410^h$			
	NV(1242)		$\leq 0.410^h$			
3044.48	CIV(1548)	0.96646	0.629	0.180	3.49	≥ 1.74
	CIV(1550)		$\leq 0.36^h$			
0454-2203		$z_{em} = 0.534$		V=16.1 ^d		
3	$z_{ave} = 0.41261, \sigma_z = 0.00025$ A,B,C ^e					
1717.28	Ly α	0.41262	0.489	0.036	13.58	0.72 ⁱ
1448.75	Ly β	0.41242	0.683	0.060	11.46	$\geq 5.85^i$
1457.61	OVI(1032)	0.41251	0.851	0.059 ^f	14.38	1.40
1466.13	OVI(1038)	0.41298	0.608	0.059	10.34	
1380.00	CIII(977)	0.41246	0.691	0.060	11.51	
1397.89	NIII(989)	0.41230	0.153	0.060	2.55	
1704.29	SiIII(1206)	0.41259	0.809	0.040	20.23	
1750.49	NV(1238)	0.41303	0.295	0.030	9.83	
	NV(1242)		$\leq 0.06^h$			
	CIV(1548)		$\leq 0.18^h$			
	CIV(1550)		$\leq 0.18^h$			

Table 4—Continued

Wavelength (Å)	ID	z_{obs}	W_{obs} (Å)	$\sigma(W)$ (Å)	SL ^b	LR ^c
1206+4557		$z_{em} = 1.158$		V=15.79 ^d		
4	$z_{ave} = 0.73385, \sigma_z = 0.00032$ A ^e					
2107.78	Ly α	0.73384	0.847	0.051	16.54	0.75
1779.34	Ly β	0.73472	1.131 ⁱ	0.081	13.96	
1789.01	OVI(1032)	0.73365	0.279	0.077	3.62	1.15
1799.50	OVI(1038)	0.73426	0.243	0.076	3.19	
	NV(1238)		$\leq 0.44^h$			
	NV(1242)		$\leq 0.44^h$			
2684.95	CIV(1548)	0.73424	0.371	0.066	5.62	
	CIV(1550)		$\leq 0.13^h$			
5	$z_{ave} = 0.92703, \sigma_z = 0.00042$ A,B,C ^e					
2342.55	Ly α	0.92696	4.490	0.122 ^f	36.80	1.50
1976.11	Ly β	0.92656	3.001	0.068 ^f	43.87	2.27
1874.54	Ly γ	0.92747	1.320	0.076 ^f	17.32	
1987.73	OVI(1032)	0.92623	2.328	0.067	34.75	0.94
1999.29	OVI(1038)	0.92680	2.490	0.067	37.16	
1881.66	CIII(977)	0.92592	4.066 ^j	0.076	53.50	
1907.79	NIII(989)	0.92745	1.113	0.078	14.27	
2294.61	SiII(1190)	0.92757	0.295	0.046	6.41	
2300.26	SiII(1193)	0.92766	0.488	0.046	10.61	
2326.10	SiIII(1206)	0.92797	1.379	0.124	11.12	
2386.94	NV(1238)	0.92679	1.792	0.117	15.32	1.64
2394.23	NV(1242)	0.92648	1.093	0.117	9.34	
2573.14	CH(1334)	0.92812	1.835	0.075	24.47	
2686.56	SiIV(1393)	0.92757	1.294	0.067	19.31	1.20
2703.75	SiIV(1402)	0.92743	1.079	0.067	16.10	
2984.04	CIV(1548)	0.92742	4.440	0.096	46.25	1.62
2988.88	CIV(1550)	0.92735	2.737	0.096	28.51	
6	$z_{ave} = 1.08275, \sigma_z = 0.00130$ A,B,C ^e					
2529.96	Ly α	1.08113	1.243	0.105	11.84	0.98
2134.35	Ly β	1.08298	1.262	0.046 ^f	27.43	2.69
2023.47	Ly γ	1.08060	0.469	0.057	8.23	
2149.35	OVI(1032)	1.08284	2.543	0.044 ^f	58.06	1.18
2161.21	OVI(1038)	1.08285	2.160	0.044 ^f	49.54	
2510.57	SiIII(1206)	1.08087	1.038	0.112	9.27	
	NV(1238)		$\leq 0.17^h$			
	NV(1242)		$\leq 0.17^h$			
3224.76	CIV(1548)	1.08291	0.605	0.101	5.98	1.20
3229.31	CIV(1550)	1.08239	0.505	0.101	5.00	

Table 4—Continued

Wavelength (Å)	ID	z_{obs}	W_{obs} (Å)	$\sigma(W)$ (Å)	SL ^b	LR ^c
1317+2743		$z_{em} = 1.022$		V=15.98 ^d		
No O VI Detected						
1352+0106		$z_{em} = 1.121$		V=16.03 ^d		
7	$z_{ave} = 0.66752, \sigma_z = 0.00034$ A,B,C ^e					
2026.88	Ly α	0.66730	2.920	0.065 ^f	45.06	1.34
1710.59	Ly β	0.66769	2.177	0.086 ^f	25.20	
1721.07	OVI(1032)	0.66782	1.089	0.084	12.90	2.46
1730.69	OVI(1038)	0.66794	0.442	0.083	5.35	
1985.62	SiII(1190)	0.66800	0.503	0.064	7.86	
1989.50	SiII(1193)	0.66724	1.084	0.064	16.94	
2011.92	SiIII(1206)	0.66757	1.652	0.065 ^f	25.41	
2066.08	NV(1238)	0.66778	0.485	0.053	9.15	1.49
2072.16	NV(1242)	0.66733	0.325	0.052	6.25	
2225.39	CII(1334)	0.66754	1.197	0.047	25.47	
2324.18	SiIV(1393)	0.66757	1.225	0.124	9.88	0.73
2338.93	SiIV(1402)	0.66737	1.681	0.123	13.67	
2581.02	CIV(1548)	0.66711	2.219	0.074	29.98	1.16
2585.92	CIV(1550)	0.66750	1.921	0.074	25.96	
1407+2632		$z_{em} = 0.944$		V=15.73 ^d		
No O VI Detected						
1424-1150		$z_{em} = 0.806$		V=16.49 ^d		
8	$z_{ave} = 0.65516, \sigma_z = 0.00027$ A,B ^e					
2012.11	Ly α	0.65514	1.959	0.083 ^f	23.72	1.58
1697.85	Ly β	0.65528	1.237	0.101 ^f	12.22	
1707.88	OVI(1032)	0.65503	0.313	0.100	3.14	0.77
1716.98	OVI(1038)	0.65473	0.409	0.098	4.16	
1997.45	SiIII(1206)	0.65557	0.299	0.083	3.60	
	NV(1238)		$\leq 0.17^h$			
	NV(1242)		$\leq 0.17^h$			
2562.81	CIV(1548)	0.65535	0.653	0.137	4.77	0.78
2567.06	CIV(1550)	0.65535	0.842	0.137	6.15	
9	$z_{ave} = 0.74654, \sigma_z = 0.00042$ A,B ^e					
2123.49	Ly α	0.74676	0.463	0.062	7.42	≥ 2.80
1801.81	OVI(1032)	0.74606	0.542	0.083	6.56	1.91
1812.53	OVI(1038)	0.74682	0.284	0.081	3.51	
	NV(1238)		$\leq 0.11^h$			
	NV(1242)		$\leq 0.11^h$			
	CIV(1548)		$\leq 0.22^h$			
	CIV(1550)		$\leq 0.22^h$			

Table 4—Continued

Wavelength (Å)	ID	z_{obs}	W_{obs} (Å)	$\sigma(W)$ (Å)	SL ^b	LR ^c
1435+6349		$z_{em} = 2.068$		V=15.0 ^d		
No O VI Detected						
1522+1009		$z_{em} = 1.321$		V=15.74 ^d		
No O VI Detected						
1634+7037		$z_{em} = 1.334$		V=14.9 ^d		
10	$z_{ave} = 1.04162, \sigma_z = 0.00017$ A,B ^e					
2481.92	Ly α	1.04161	2.731	0.037 ^f	74.21	1.94
2094.08	Ly β	1.04157	1.411	0.052 ^f	27.34	1.37
1985.50	Ly γ	1.04156	1.032	0.068	15.09	1.05
1939.12	Ly δ	1.04174	0.983	0.073	13.43	1.25
1914.87	Ly ϵ	1.04187	0.786	0.078	10.08	
2107.08	OVI(1032)	1.04188	0.424	0.049	8.58	1.48
2118.31	OVI(1038)	1.04151	0.287	0.049	5.86	
1994.39	CIII(977)	1.04130	0.406	0.067	6.06	
2430.49	SiII(1190)	1.04172	0.258	0.067	3.85	
2436.10	SiII(1193)	1.04150	1.532	0.037	41.85	
2463.84	SiIII(1206)	1.04214	1.121	0.037	30.29	
	NV(1238)		$\leq 0.07^h$			
	NV(1242)		$\leq 0.07^h$			
2724.81	CII(1334)	1.04178	0.216	0.031	6.92	
3160.21	CIV(1548)	1.04122	1.044	0.036	28.83	1.41
3165.87	CIV(1550)	1.04148	0.743	0.036	20.52	
11	$z_{ave} = 1.14121, \sigma_z = 0.00028$ A,B ^e					
2602.99	Ly α	1.14120	1.088	0.033	32.52	6.26
2196.12	Ly β	1.14105	0.174	0.048	3.65	≥ 1.61
2209.94	OVI(1032)	1.14156	0.242	0.047	5.19	1.20
2222.08	OVI(1038)	1.14152	0.202	0.046	4.42	
	NV(1238)		$\leq 0.07^h$			
	NV(1242)		$\leq 0.07^h$			
2698.25	SiII(1260)	1.14075	0.533	0.032	16.66	

Table 4—Continued

Wavelength (Å)	ID	z_{obs}	W_{obs} (Å)	$\sigma(W)$ (Å)	SL ^b	LR ^c
2340-0340		$z_{em} = 0.896$		V=16.02 ^d		
12	$z_{ave} = 0.68416, \sigma_z = 0.00029$ A,B ^e					
2047.22	Ly α	0.68403	1.764	0.065	26.97	0.94 ⁱ
1727.90	Ly β	0.68457	1.882	0.094	19.94	5.88 ⁱ
1637.57	Ly γ	0.68381	0.320	0.134	2.39	
1737.92	OVI(1032)	0.68415	0.525	0.093	5.62	1.68
1747.65	OVI(1038)	0.68428	0.312	0.092	3.39	
1645.67	CIII(977)	0.68438	1.657	0.127	13.05	
2031.65	SiIII(1206)	0.68392	0.466	0.067	6.96	
2086.02	NV(1238)	0.68388	0.148	0.062	2.39	≥ 1.19
	NV(1242)		$\leq 0.12^h$			
2247.02	CH(1334)	0.68375	0.201	0.044	4.57	

^a Table contains 11 Objects, 20 Spectra, & 12 O VI detections.

^b Significance Level: $W_{obs}/\sigma(W)$.

^c Line Ratio: Ratio of equivalent widths is calculated for the following pairs of lines. (Ly α /Ly β , Ly β /Ly γ , O VI(1032)/O VI(1038), N V(1238)/N V(1242), C IV(1548)/C IV(1550)). Ratio is listed with stronger line. If weaker line is not detected above the 2σ equivalent width limit, then that limit is used in the Line Ratio.

^d Visual Magnitude

^e z_{ave} is calculated as the weighted mean of Ly α , Ly β , Ly γ , O VI(1032) & O VI(1038). See text for a description of the weighting procedure. Standard deviation is calculated for the five lines above. The samples in which the system has been included are marked by the letters A,B,C.

^f This line had an upper limit, described in the text, used in place of its Significance Level as the weight for calculating z_{ave} .

^g O VI(1032) at $z_{abs} = 0.9534$ is blended with Ly β at $z_{abs} = 0.9669$.

^h Absorption due to this ion is not detected at the 2σ level at z_{ave} . An upper limit equal to the 2σ equivalent width level is listed.

ⁱ The line ratio does not fall within the 1σ error of the theoretical prediction.

^j This line is blended producing excess equivalent width.

QSO	z_{abs}	Rest Equivalent Widths (Å)			Doublet Ratio	
		O VI	O VI	C II	Subtracted ^b	Fitted ^c
		1032	1036-8 ^a	1334		
0122-0021	0.9534	0.62	0.44	0.18	2.00 ^d	1.40
	0.9669	0.36	0.25	≤ 0.16	1.44	1.44
0454-2203	0.4126	0.60	0.43	≤ 0.02	1.40	1.40
1206+4557	0.7339	0.16	0.14	≤ 0.11	1.14	1.15
	0.9270	1.21	1.29	≤ 0.11	0.94	0.94
	1.0828	1.22	1.04	≤ 0.10	1.17	1.18
1352+0106	0.6675	0.65	0.85	0.72	1.98 ^d	2.46
1424-1150	0.6552	0.19	0.25	≤ 0.09	0.76	0.76
	0.7465	0.31	0.16	≤ 0.17	1.94	1.91
1634+7037	1.0416	0.21	0.17	0.10	1.96 ^d	1.48
	1.1412	0.11	0.09	≤ 0.03	1.22	1.20
2340-0340	0.6842	0.31	0.35	0.12	1.37 ^d	1.68

Table 5: Doublet Ratios

^a Rest equivalent width including both O VI(1038) and C II(1036).

^b W(1032)/W(1038), corrected for C II(1036) when C II(1334) was detected.

^c W(1032)/W(1038), using W for O VI (1038) deblended from C II(1036) in Table 4.

^d Doublet ratio corrected for calculated C II(1036).

QSO	z_{abs}	Oxygen VI ^b		Carbon IV ^c		Hydrogen I ^d	
		Log(N)	b	Log(N)	b	Log(N)	b
		cm ⁻²	km s ⁻¹	cm ⁻²	km s ⁻¹	cm ⁻²	km s ⁻¹
0122-0021	0.9534	15.1 ^{+0.3} _{-0.3}	74 ⁺⁷⁰ ₋₂₅	15.3 ^{+2.3} _{-0.5}	54 ⁺²⁸ ₋₂₀	17.0 ^{+1.5} _{-0.5}	53 ⁺¹⁰ ₋₁₃
	0.9669	14.8 ^{+1.3} _{-0.2}	45 ⁺¹⁰⁰ ₋₂₆	13.9 ^e	...	16.1 ^{+0.4} _{-0.2}	49 ⁺⁸ ₋₉
0454-2203	0.4126	15.1 ^{+0.2} _{-0.2}	70 ⁺³⁹ ₋₂₀	≤ 13.5 ^g ^f	... ^f
1206+4557	0.7339	... ^f	... ^f	13.7 ^e ^f	... ^f
	0.9270	... ^f	... ^f	15.0 ^{+0.1} _{-0.1}	223 ⁺⁴⁵ ₋₁	18.7 ^{+0.9} _{-0.7}	86 ⁺⁹ ₋₁₀
	1.0828	15.7 ^{+0.2} _{-0.1}	106 ⁺¹⁰ ₋₁₀	... ^f	... ^f	... ^f	... ^f
1352+0106	0.6675	14.7 ^e	...	15.3 ^{+0.7} _{-0.2}	74 ⁺¹³ ₋₁₈	... ^f	... ^f
1424-1150	0.6552	... ^f	... ^f	... ^f	... ^f	17.8 ^{+2.0} _{-0.9}	49 ⁺⁶ ₋₁₆
	0.7465	14.4 ^e	...	≤ 13.5 ^g	...	13.7 ^e	...
	1.0416	14.8 ^{+1.3} _{-0.5}	20 ⁺⁵⁰ ₋₁₀	14.5 ^{+0.1} _{-0.1}	40 ⁺¹¹ ₋₇	16.6 ^{+0.2} _{-0.1}	63 ⁺³ ₋₃
1634+7037	1.1412	14.6 ^{+1.7} _{-0.5}	10 ⁺³⁰ ₋₄	15.1 ^{+0.2} _{-0.2}	31 ⁺³ ₋₃
	2340-0340	14.6 ^{+1.4} _{-0.2}	45 ^{+∞} ₋₃₂ ^f	... ^f

Table 6: Column Densities and Dispersion Velocities^a

^a Values are calculated with two equivalent width measurements and their 1σ errors.

^b From lines $\lambda\lambda 1032, 1038$.

^c From lines $\lambda\lambda 1548, 1550$.

^d From lines $\lambda 1215, \lambda 1025$.

^e Doublet ratio suggests linear absorption. Column density estimate is based on the stronger member.

^f Absorption lines are too saturated to be effectively analyzed in with the doublet ratio method.

^g Neither line was detected above 2σ . Upper limit is placed on column density assuming linear absorption.

Object	z_{abs}	W(1032)	W(1025)	R_{OB}	$\sigma_{R_{OB}}$	W(1548)	R_{OC}	$\sigma_{R_{OC}}$
0122-0021	0.9534	1.21	1.37	0.88	0.10	1.99	0.56	0.07
	0.9669	0.71	0.80	0.89	0.16	0.63	1.13	0.36
0454-2203	0.4126	0.85	0.68	1.25	0.14	$\leq 0.07^a$	≥ 12.1	...
1206+4557	0.7339	0.28	$\leq 0.85^b$	0.33	0.09	0.37	0.76	0.25
	0.9270	2.32	3.00	0.77	0.03	4.44	0.53	0.02
	1.0828	2.54	1.26	2.02	0.08	0.61	4.17	0.71
1352+0106	0.6675	1.09	2.18	0.50	0.05	2.22	0.49	0.04
1424-1150	0.6552	0.31	1.24	0.25	0.08	0.65	0.48	0.19
	0.7465	0.54	$\leq 0.17^c$	≥ 3.18	...	$\leq 0.27^a$	≥ 2.00	...
1634+7037	1.0416	0.42	1.41	0.33	0.04	1.04	0.40	0.05
	1.1412	0.24	0.17	1.41	0.48	$\leq 0.07^a$	≥ 3.4	...
2340-0340	0.6842	0.53	1.88	0.28	0.08	$\leq 0.32^a$	≥ 1.7	...

Table 7: Ion Ratios

^a C IV(1548) is not detected, an upper limit 2σ equivalent width is listed.

^b Ly β is apparently blended with another Ly α line; an upper limit of the equivalent width is given by its corresponding Ly α .

^c Ly β is not detected, an upper limit 2σ equivalent width is listed.

REFERENCES

- Anders, E., & Grevesse, N. 1989, *Geochim. Cosmochim. Acta*, 53, 197
- Bahcall, J. N., Bergeron, J., Boksenberg, A., Hartig, G. F., Jannuzi, B. T., Kirhakos, S., Sargent, W. L. W., Savage, B. D., Schneider, D. P., Turnshek, D. A., Weymann, R. J., & Wolfe, A. 1993, *ApJS*, 87, 1
- Barcons, X., Fabian A. C., & Rees, M. J. 1991, *Nature*, 350, 685
- Bergeron, J., Petitjean, P., Sargent, W. L. W., Bahcall, J. N., Boksenberg, A., Hartig, G. F., Jannuzi, B. T., Kirhakos, S., Savage, B. D., Schneider, D. P., Turnshek, D. A., Weymann, R. J., & Wolfe, A. 1994, *ApJ*, 436, 33
- Bergeron, J. 1988, in *QSO Absorption Lines: Probing the Universe*, ed. J. C. Blades, D. A. Turnshek, & C. A. Norman (Cambridge: Cambridge Univ. Press), 127
- Burrows, D. N., & Mendenhall, J. A. 1991, *Nature*, 351, 629
- Cohen, R. D., Bartko, F., Beaver, E. A., Burbidge, E. M., Junkkarinen, V. T., Lyons, R. W., Rosenblatt, E. I., Burks, G. S., Harms, R. J., & Henriksen, M. 1991, *BAAS*, 23 1426
- Cox, D. P., & Tucker, W. H. 1969, *ApJ*, 157, 1157
- Davidson, A. F., Bowers, C. W., Kruk, J. W., Kriss, G. A., Ferguson, H. C., Blair, W. P., Kimble, R. A., & Long, K. S. 1991, *BAAS*, 23, 1472
- Fabbiano, G. 1989, *ARA&A*, 27, 87
- Fan, L., & Ikeuchi, S. 1992, *ApJ*, 390, 405
- Fan, X.-M. 1995, Ph.D. Thesis, Columbia University
- Forman, W., Schwarz, J., Jones, C., Liller, W., & Fabian, A. C. 1979, *ApJL*, 234, L27
- Gnedin, N. Y., & Ostriker, J. P. 1992 *ApJ* 400, 1
- Hamann, F., Barlow, T. A., Beaver, E. A., Burbidge, E. M., Cohen, R. D., Junkkarinen, V., & Lyons, R. 1995, *ApJ*, 443, 606
- Hamann, F., Zuo, L., & Tytler, D. 1995, Submitted to *ApJ*
- Hartquist, T. W., & Snijders, M. A. J. 1982, *Nature*, 299, 783
- Jakobsen, P., Boksenberg, A., Deharveng, J. M., Greenfield, P., Jedrzejewski, R., & Paresce, F. 1994, *Nature*, 370, 35
- Lanzetta, K. M., Turnshek, D. A., & Wolfe, A. M. 1987, *ApJ*, 322, 739
- Lanzetta, K. M., Wolfe, A. M., Turnshek, D. A., Lu, L., McMahon, R. G., & Hazard, C. 1991, *ApJS*, 77, 1
- Lu, L., & Savage, B. D. 1993, *ApJ*, 403, 127
- Madua, P. 1994, private communication
- Morton, D. C. 1991, *ApJS*, 77, 119
- Pettini, M., & D’Odorico, S. 1986, *ApJ*, 310, 700
- Reimers, D., et al. 1992, *Nature*, 360, 561

- Sargent, W. L. W., Steidel, C. C., & Boksenberg A. 1989, ApJS, 69, 703
- Sargent, W. L. W., Boksenberg, A., & Steidel, C. C. 1990, ApJS, 68, 539
- Schneider, D. P., Hartig, G. F., Jannuzi, B. T., Kirhakos, S., Saxe, D. H., Weymann, R. J., Bahcall, J. N., Bergeron, J., Boksenberg, A., Sargent, W. L. W., Savage, B. D., Turnshek, D. A., & Wolfe, A. 1993, ApJS, 87, 45
- Sembach, K. R., & Savage, B.D. 1992, ApJS, 83, 147
- Shapiro, P. R., & Moore, R. T. 1976, ApJ, 207, 460
- Shapiro, P. R., & Benjamin, R. 1991 PASP, 103, 923
- Snowden, S. L., Mebold, U., Hirth, W., Herbstmeier, U., & Schmitt, J. H. M. M. 1991, Science, 252, 1529
- Songaila, A., Cowie, L. L., Hogan, C. J., & Rugers, M. 1994 Nature, 368, 599
- Spitzer, L. 1978, Physical processes in the interstellar medium, (New York:Wiley), p.44
- Steidel, C. C., 1990, ApJS, 74, 37
- Tytler, D., & Fan, X. M. 1994 BAAS, 27, 1424
- Tytler, D., Boksenberg, A., Sargent, W. L. W., Young, P., & Kunth, D. 1987, ApJS, 64, 667
- Verner, D. A., Barthel, P. D., & Tytler, D. 1994, A&AS, 108, 287
- Verner, D. A., Tytler, D., & Barthel, P. D. 1994, ApJ, 430, 186 (VTB94)
- Verner, D. A., & Yakolev, D. G. 1990, Ap&SS, 165, 27
- Wang, Q. 1991, ApJL, 377, L85
- Wolfe, A. M., Turnshek, D. A., Smith, H. E., & Cohen, R. D. 1986, ApJS, 61, 249
- Wolfe, A. M., Lanzetta, K. M., Foltz, C. B., & Chaffee, F. H. 1995, ApJ, submitted
- Wright, E.L., Mather, J.C., Fixsen, D.J., Kogut, A., Shafer, R. A., Bennett, C. L., Boggess, N. W., Cheng, E. S., Silverberg, R. F., Smoot, G. F., & Weiss, R. 1994 ApJ, 420, 450
- Young, P. J., Sargent, W. L. W., Boksenberg, A., Carswell, R. F., & Whelan, J. A. J. 1979, ApJ, 229, 891

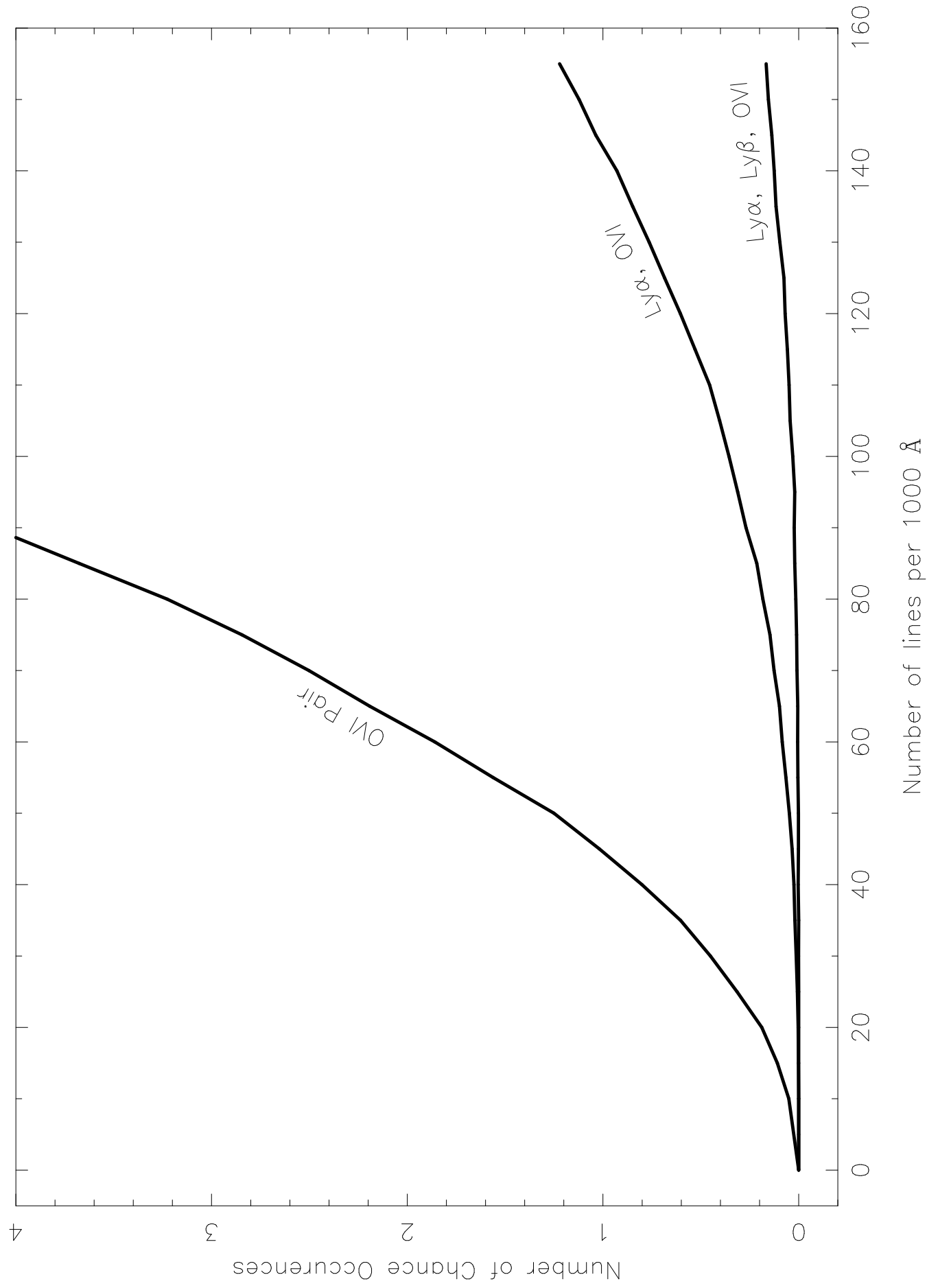
Fig. 1.— Number of chance coincidences of new redshift systems with two lines (O VI pairs), three lines (Ly α and O VI), and four lines (Ly α , Ly β and O VI). We used a random distribution of lines, and accepted lines into a system if the redshift for each line fell within $\Delta z = 0.0005$ of all the others. We see that the number of false three lined systems is about 10% that of the two lined systems. Each HST spectrum covers 700 – 1000 Å, the real lines density is 80.0 per 1000 Å in the Lyman- α forest, and real O VI systems occur about 1 per 1000 Å in the rest frame. Therefore, we require at least 3 lines per system in order to avoid excessive coincidences.

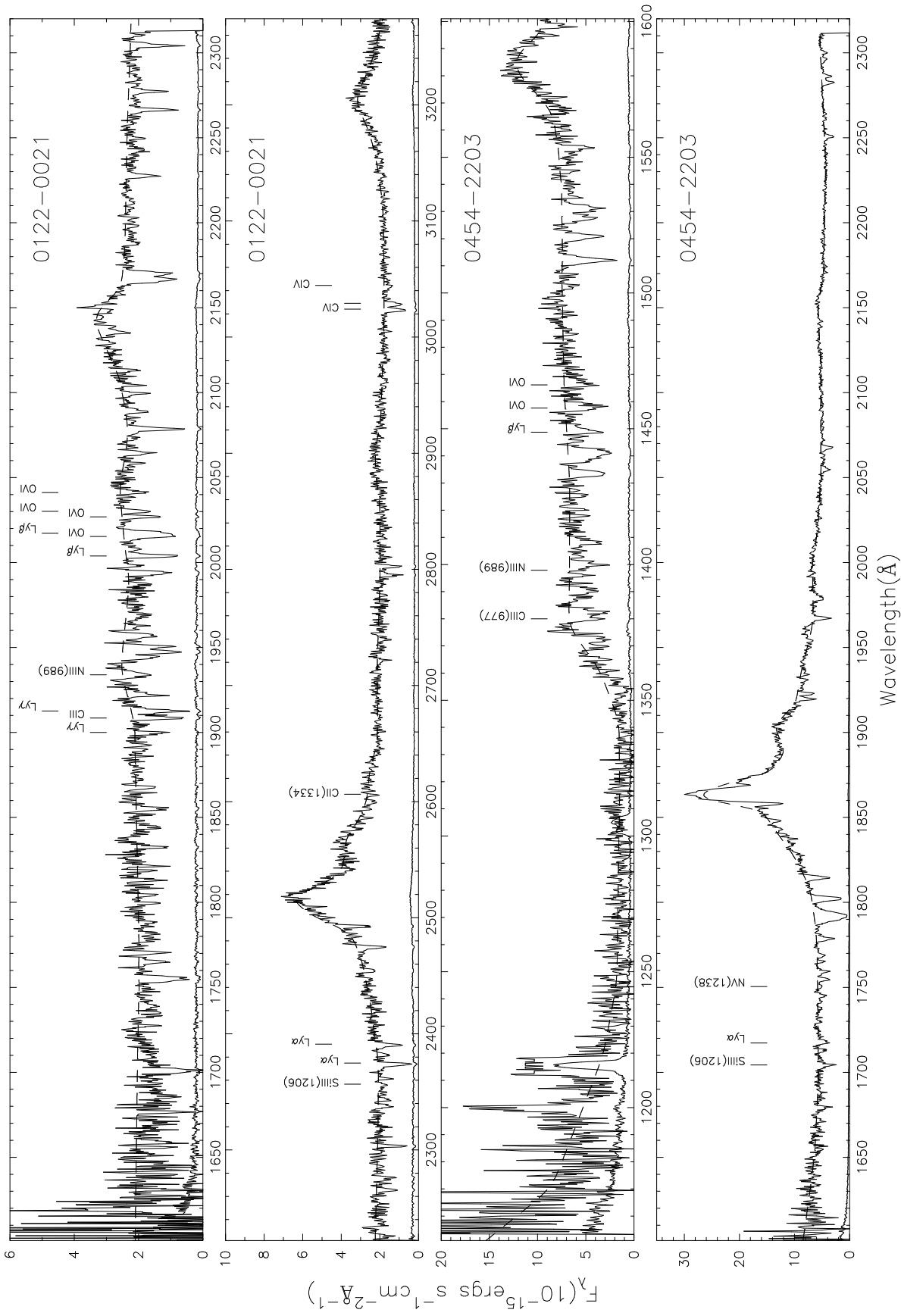
Fig. 2.— The spectra of 11 QSOs plotted with the fitted continuum and 1σ error. Lines identified with Oxygen VI absorption systems are labeled (see Table 4). Labels of the same height indicate lines of a common system.

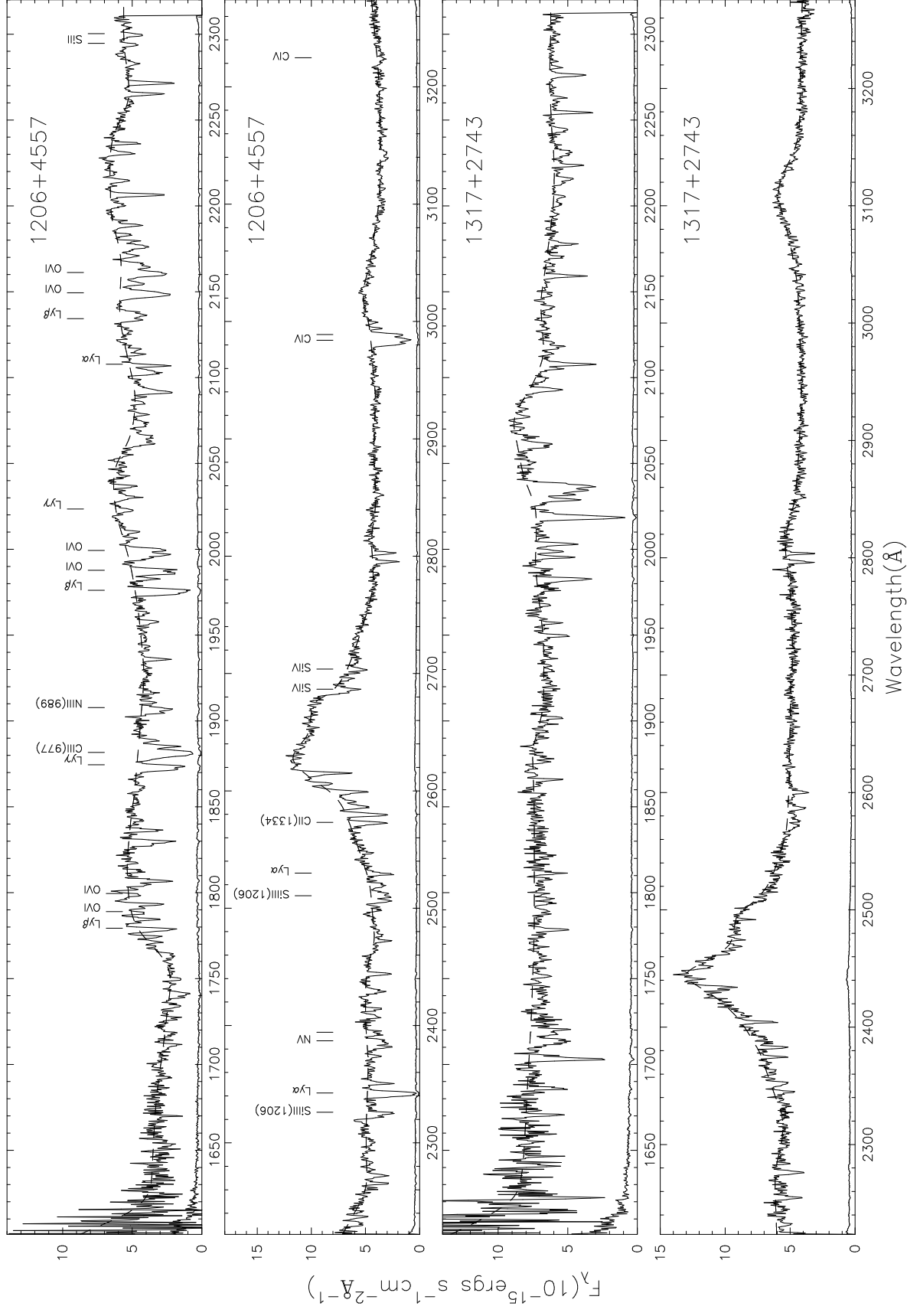
Fig. 3.— Plots of Lyman- α , Lyman- β , O VI, and C IV absorption in velocity space for each of the 12 systems in which O VI was identified. Zero velocity corresponds to the z_{abs} indicated for each system. Flux scales are different depending on the strength of absorption.

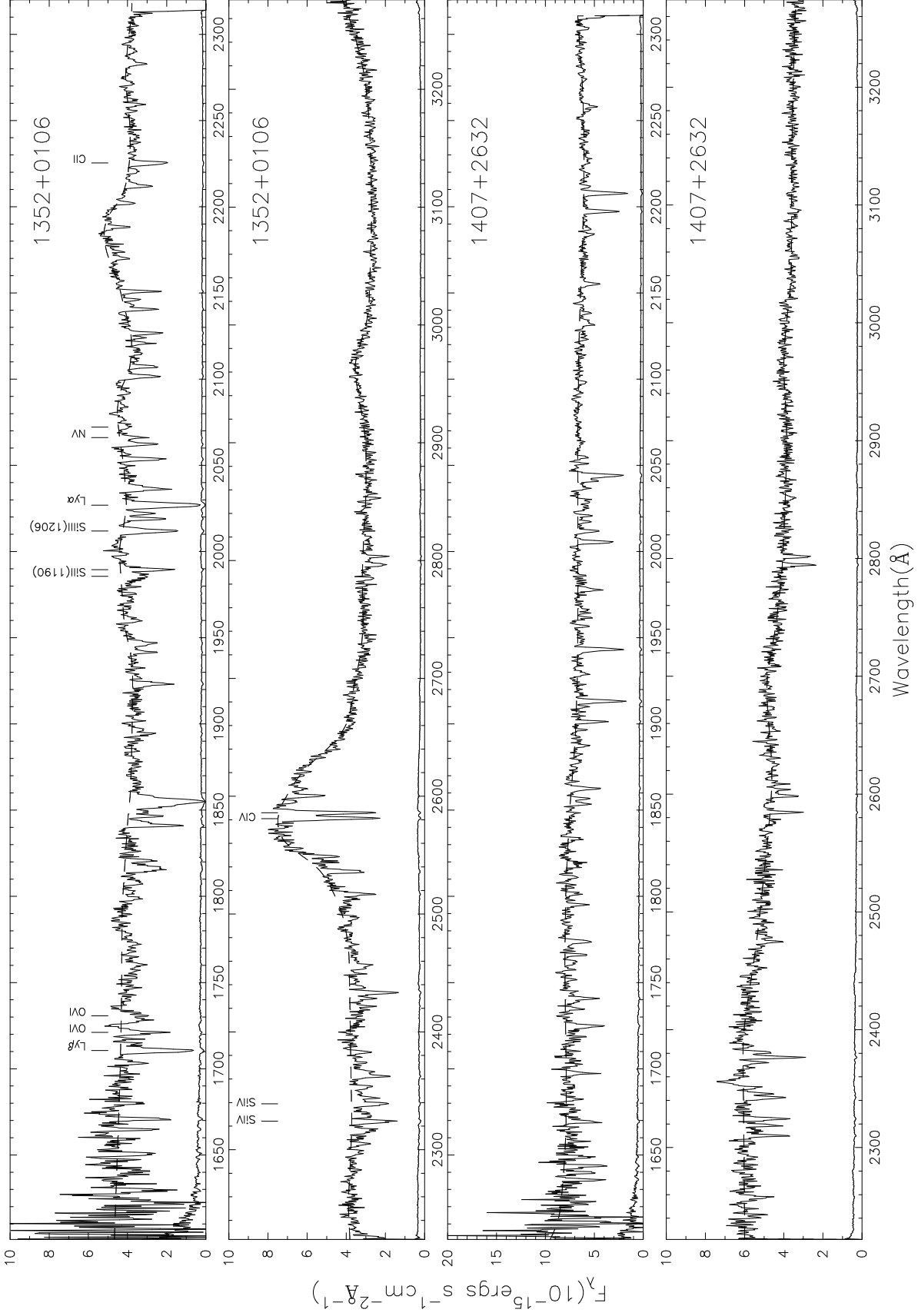
Fig. 4.— Calculated O VI Doublet Ratio versus Column Density for a single absorbing cloud. Our search was sensitive to the right of the vertical dashed line at $\log(N_{OVI}) > 14.5$, which corresponds to $W(1038) > 0.21$ Å.

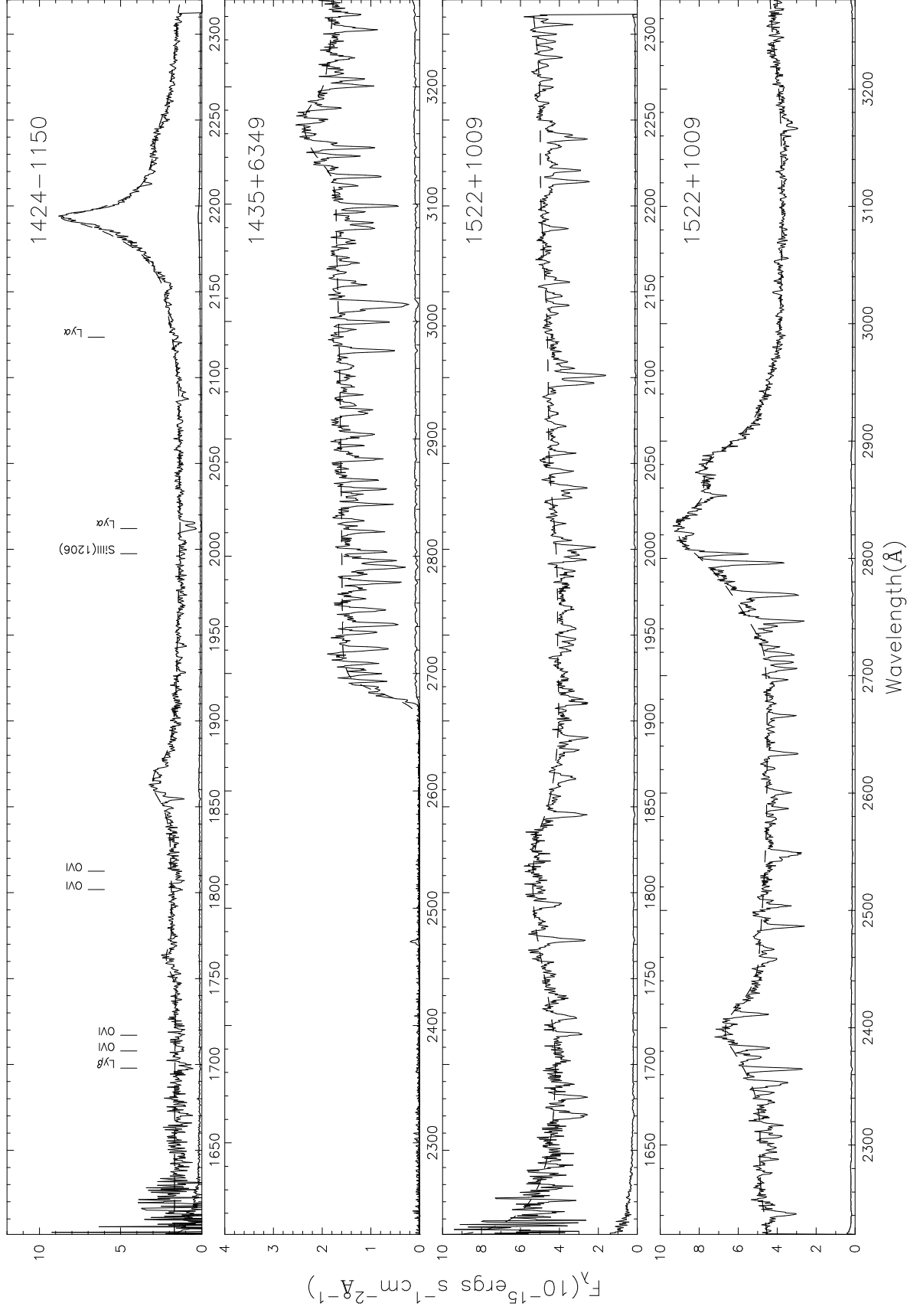
Fig. 5.— Equivalent width ratios for the 12 systems in Sample A. Ratios of equivalent widths and the 1σ error are calculated in each system where absorption was detected at the respective wavelengths. Lower limits are shown with arrows in the systems where C IV or Ly β are not detected.

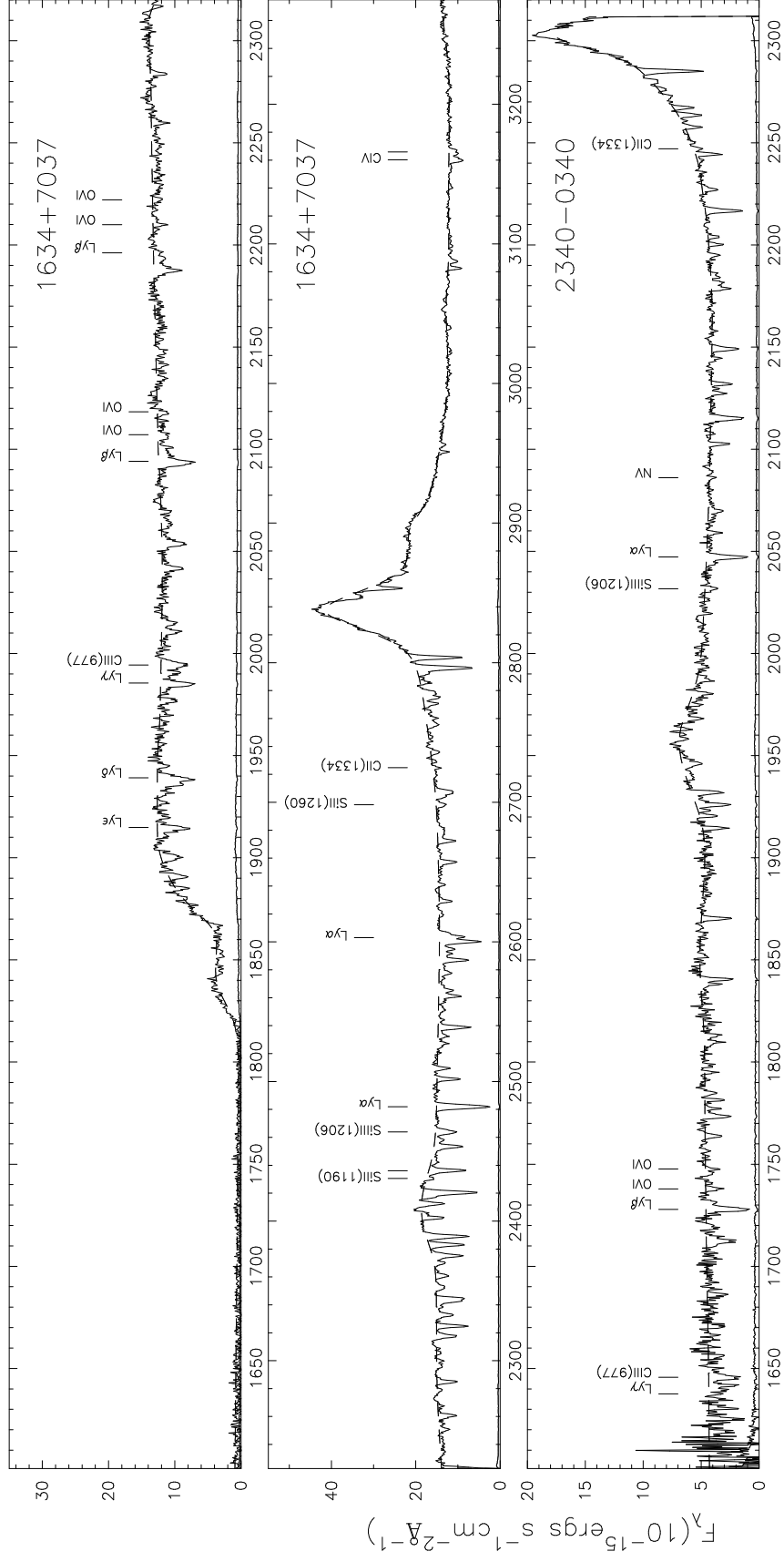












Wavelength(\AA)

